Entanglement generation and detection in split exciton-polariton condensates

Jingyan Feng [1], Hui Li,[1] Zheng Sun,[1] and Tim Byrnes[1,2,3,4,5,6,*]

[1]*State Key Laboratory of Precision Spectroscopy, School of Physical and Material Sciences, East China Normal University, Shanghai 200062, China*

[2]*New York University Shanghai, 567 West Yangsi Road, Shanghai 200126, China*

[3]*NYU-ECNU Institute of Physics, NYU Shanghai, 3663 Zhongshan Road North, Shanghai 200062, China*

[4]*Shanghai Frontiers Science Center of Artificial Intelligence and Deep Learning, NYU Shanghai, 567 West Yangsi Road, Shanghai 200126, China*

[5]*Center for Quantum and Topological Systems, NYUAD Research Institute, New York University Abu Dhabi, Abu Dhabi, United Arab Emirates*

[6]*Department of Physics, New York University, New York, New York 10003, USA*

We propose a method of generating and detecting spatially defined entanglement in exciton-polariton condensates at steady state. In our scheme we first create a spinor polariton condensate, such that steady-state squeezing is obtained under a one-axis twisting interaction. Then the condensate is split either physically or virtually, which results in entanglement generated between the two parts. A virtual split means that the condensate is not physically split, but its near-field image is divided into two parts, and the spin correlations are deduced from polarization measurements in each half. We theoretically model and examine the logarithmic negativity criterion and several correlation-based criteria to show that entanglement exists under experimentally achievable parameters.

I. INTRODUCTION

Entanglement is a central property of quantum physics that distinguishes it from classical physics [1,2] and is considered an essential resource for applications such as quantum information [3,4], quantum cryptography [5–7], and quantum metrology [8,9]. Entangled states have already been achieved at the macroscopic scale and in systems such as atomic ensembles [10] and mechanical resonators [11]. Several experiments realized the generation of entanglement and other quantum correlations in a single Bose-Einstein-condensate (BEC) cloud [12–15], which has been proposed for several applications [16,17]. A well-known platform for creating BECs is to use suitably structured semiconductor systems supporting exciton-polaritons. Exciton-polaritons are a superposition of an exciton (an electron-hole bound pair) and a cavity photon and form a bosonic quasiparticle [18–21]. The coupling between the exciton and photon results in an extremely light mass for the exciton-polaritons [21,22], allowing for the possibility of realizing BECs [19,22–25]. One of the advantages of polariton BECs is that they can be experimentally implemented at higher temperatures, even at room temperatures, by using materials such as GaN and ZnO [26–31]. This makes the polariton system attractive for future technological applications, as they would not require a bulky cryogenic apparatus.

Recently, it was observed that entanglement between two spatially separated atomic BECs could be generated [32]. In that study, the authors first created a spinor ^{87}Rb BEC via spin squeezing, which generates Einstein-Podolsky-Rosen (EPR) multiparticle entanglement in the single BEC. Next, the single BEC was physically split into two parts, and the EPR entanglement between the two components was verified by measuring spin correlations. Prior to this, entanglement between different spatial regions of atomic BECs was achieved [12–14]. In these works, entanglement was first created between the atoms on a single ^{87}Rb atomic BEC, using methods such as state-dependent forces, spin-nematic squeezing, and spin-changing collisions. Then, by using a magnified near-field image of the single atomic BEC, two different spatial regions of the same BEC were examined for correlations. It was shown that entanglement can be detected after releasing the atomic gases from the traps. These experimental works showed that the splitting process can be either virtual or physical, in which coherence and entanglement can still survive after the split. The physical-splitting scheme [32] requires precise techniques to avoid environment noise to avoid additional sources of decoherence. However, as shown in Ref. [33], physical and virtual splits give identical results in terms of entanglement. Thus, the virtual-splitting procedure may be an excellent option for observing such entanglement, even if physical splitting is closer to the concept of "splitting." We note that numerous theoretical proposals also have been made for generating entanglement in two completely separate atomic BECs [33–41]. For polariton condensates, to date, no reports of detection of entanglement in single or multiple polariton condensates have been made. However, squeezing in the polaritonic system has been observed [42], in which the quadrature squeezing in polaritons is generated by using a four-wave mixing method. Furthermore, experimental quantum optical toolbox techniques were developed for polaritonic systems such as homodyne detection in Ref. [42].
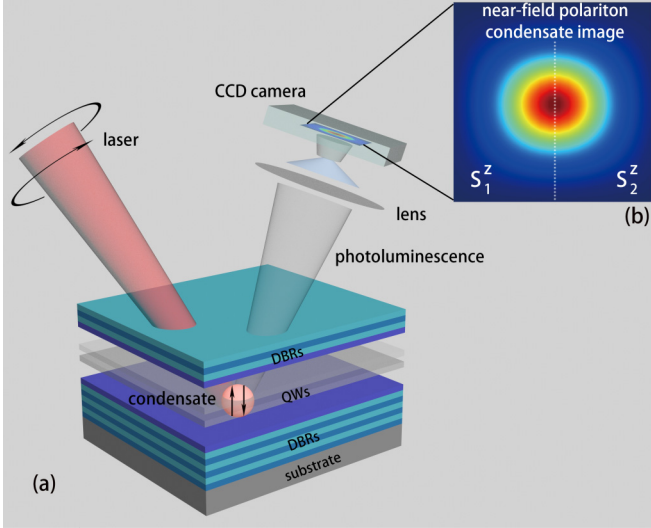
*tim.byrnes@nyu.edu

FIG. 1. The experimental setup for our system. (a) A spinor exciton-polariton condensate forms in the QWs generated by the pump laser. The spinor condensate is formed from the spin components of the polaritons and is excited by applying a laser of suitable polarization (both clockwise and counterclockwise circular polarization) to excite equal populations of the spins. The photon component of the polaritons leaks through the semiconductor quantum microcavity; then its image is focused on a charge-coupled device (CCD) of a camera. By individually detecting the polarization of the separate parts of the photoluminescence (imaged light) on a CCD, one may deduce the presence of entanglement between different spatial regions of the condensate as imaged on the CCD. (b) The enlarged image resolved from the CCD. The vertical dashed line shows the regions defining the two spin components used to detect entanglement.

These results make the probability that such entanglement splitting in two polariton condensates can be realized in the near future promising, taking advantage of the fact that such systems can be easily manipulated [43–45].

In this paper, we propose a method of generating entanglement in a split polariton condensate and give an experimental scheme for detecting entanglement (see Fig. 1). A single spinor polariton condensate is initially excited in the QWs by optical pumping. Due to the natural self-interactions between the polaritons, this produces a one-axis twisting effect, producing multiparticle entanglement which involves all polaritons in the condensate. The single condensate is then spatially split into two ensembles which produce two separate spins. We note that this splitting procedure can be either a physical split or a virtual-splitting procedure, where the image of the polaritons is partitioned into two [Fig. 1(b)] [33]. After the splitting procedure, the subsystems are still entangled due to the one-axis twisting producing multiparticle entanglement (see Fig. 2) [46–48]. We use a spin mapping to map our system with particle-number fluctuations onto a fixed-particle-number space in order to use well-established spin correlators developed to detect entanglement. We calculate logarithmic negativity and correlation-based criteria to demonstrate that multiparticle entanglement exists not only in each condensate but in a spatially separated configuration
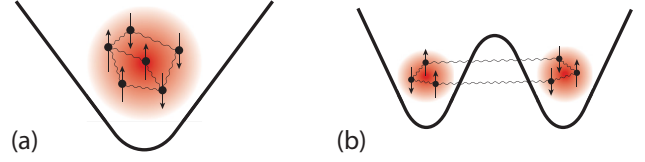

FIG. 2. Entanglement in a split polariton condensate. (a) A single spinor polariton condensate first forms in the QWs, generating multiparticle entanglement at steady state, represented by the wiggly lines. (b) The external potential trapping the condensate is modified such that it is spatially split into two condensates. The entanglement is transformed to a nonlocal form where it exists between the two split condensates.

between two condensates. We show that our system exhibits stronger entanglement for larger particle-number sectors in various regimes. By adjusting realistic system parameters one can improve the entanglement level.

This paper is organized as follows. In Sec. II we introduce the theoretical model for a single spinor exciton-polariton condensate and introduce the splitting operation, which produces two spatially separate condensates. In Sec. III, we numerically simulate our method and analyze our simulation results. In Sec. IV, we show the main results of entanglement generation and detection using different entanglement criteria. Finally, in Sec. V we summarize and discuss our results.

II. SPIN-SQUEEZED POLARITON CONDENSATES

A. Theoretical model

We now describe the theoretical model used to simulate our interacting spinor polariton condensate. For further details we refer the reader to Ref. [49], which analyzes a similar situation prior to splitting. The master equation for the spinor polariton condensate is

$$\frac{d\rho}{dt} = -\frac{i}{\hbar}[H_{\text{system}}, \rho] - \frac{\gamma}{2}\mathcal{L}[a, \rho] - \frac{\gamma}{2}\mathcal{L}[b, \rho], \quad (1)$$

where the Hamiltonian $H_{\text{system}} = H_0 + H_{\text{pump}} + H_{\text{int}}$ is defined as

$$H_0 = \hbar\Delta(a^\dagger a + b^\dagger b),$$

$$H_{\text{pump}} = \hbar A(a^\dagger e^{-i\theta_a} + a e^{i\theta_a} + b^\dagger e^{-i\theta_b} + b e^{i\theta_b}),$$

$$H_{\text{int}} = \frac{\hbar U}{2}[a^\dagger a(a^\dagger a - 1)] + \frac{\hbar U}{2}[b^\dagger b(b^\dagger b - 1)]$$
$$+ \hbar V a^\dagger a b^\dagger b. \quad (2)$$

Here, $a^\dagger$, $b^\dagger$ and a, b are the creation and annihilation operators for the two zero-momentum polariton spin species $s = \pm 1$, respectively, which obey the bosonic commutation relations

$$[a, a^\dagger] = [b, b^\dagger] = 1,$$
$$[a, b] = 0. \quad (3)$$

The contribution of higher-momentum polariton modes is not considered in our proposal because they do not affect the spin-squeezing entanglement, which is the focus of this study. The above Hamiltonian models resonant excitation, in

which the polaritons are typically excited at zero in-plane momentum, such that the remaining momenta are relatively unpopulated. One may also consider off-resonant excitation, in which other momenta will also be present, but in such a scheme only the zero-momentum polaritons should be examined, which could be achieved by filtering in momentum space. We note that resonant-excitation techniques have been used in numerous experimental studies of polariton condensates and are considered to be an equivalent way of obtaining a condensed polariton cloud, although they lack the condensation step that characterizes the condensate phase transition [42,50,51]. The Hamiltonian H_0 defines the energy $\hbar\Delta$ of zero-momentum polaritons with respect to the pump laser. H_{pump} is the Hamiltonian for the pump laser with amplitude A, and θ_a and θ_b represent the pumping phases of modes a and b, respectively. The Hamiltonian H_{int} includes the nonlinear interaction energy $\hbar U$ between the same spins and $\hbar V$ between different spins. The superoperator

$$\mathcal{L}[a, \rho] = a^\dagger a \rho + \rho a^\dagger a - 2a\rho a^\dagger,$$
$$\mathcal{L}[b, \rho] = b^\dagger b \rho + \rho b^\dagger b - 2b\rho b^\dagger \quad (4)$$

is the Lindbladian loss for photons leaking through the cavity. According to the master equation (1), the polariton population decays with rate γ.

To solve the master equation, we decompose the density matrix in the Fock basis and numerically evolve the master equation. The density matrix can be written as

$$\rho = \sum_{klk'l'} \rho_{klk'l'} |k, l\rangle\langle k', l'|, \quad (5)$$

where

$$|k, l\rangle = \frac{(a^\dagger)^k (b^\dagger)^l}{\sqrt{k!l!}} |0\rangle \quad (6)$$

are the normalized Fock states that obey $\langle k, l|k', l'\rangle = \delta_{kk'}\delta_{ll'}$.

B. Splitting the polariton condensate

Initially, spin modes a and b form a single condensate with all polaritons forming a multipartite entangled state due to the nonlinear interaction, as illustrated in Fig. 2(a). In order to obtain submodes a_1, a_2, b_1, and b_2 of spins a and b, we apply the transformation

$$a \rightarrow \frac{1}{\sqrt{2}}(a_1 + a_2),$$
$$b \rightarrow \frac{1}{\sqrt{2}}(b_1 + b_2). \quad (7)$$

The above splitting implies that there exist unoccupied modes undergoing the transformation

$$\tilde{a} \rightarrow \frac{1}{\sqrt{2}}(a_1 - a_2),$$
$$\tilde{b} \rightarrow \frac{1}{\sqrt{2}}(b_1 - b_2). \quad (8)$$

This transformation corresponds to a coherent splitting process similar to that shown in Fig. 2(b). Alternatively, it could correspond to virtual splitting like that shown in Fig. 1, where

the polariton condensate is split into two parts according to two spatial regions. These spatial regions have a one-to-one relation to the optical modes that emerge from the microcavity and hence may be spatially imaged according to the scheme shown in Fig. 1(b). The above splitting operation forms either two physically separate condensates or two distinct halves of a condensate and changes the entanglement structure, which we show in Fig. 2(b). After the split, the Fock states transform as

$$|k, l\rangle \rightarrow \frac{1}{\sqrt{k!l!}} \left(\frac{a_1^\dagger + a_2^\dagger}{\sqrt{2}}\right)^k \left(\frac{b_1^\dagger + b_2^\dagger}{\sqrt{2}}\right)^l |0\rangle$$

$$= \frac{1}{\sqrt{2^{k+l}}\sqrt{k!l!}} \sum_{nm} \binom{k}{n}\binom{l}{m}$$

$$\times (a_1^\dagger)^n (a_2^\dagger)^{k-n} (b_1^\dagger)^m (b_2^\dagger)^{l-m} |0\rangle$$

$$= \frac{1}{\sqrt{2^{k+l}}} \sum_{nm} \sqrt{\binom{k}{n}\binom{l}{m}} |n, m, k-n, l-m\rangle, \quad (9)$$

where the normalized Fock state with four modes can be written as

$$|k_1, l_1, k_2, l_2\rangle = \frac{(a_1^\dagger)^{k_1} (b_1^\dagger)^{l_1} (a_2^\dagger)^{k_2} (b_1^\dagger)^{l_2}}{\sqrt{k_1!l_1!k_2!l_2!}} |0\rangle. \quad (10)$$

Substituting the above equation into (5), the density matrix of the split condensate is written, in general, as

$$\rho^{\text{sp}} = \sum_{\substack{kl \\ k'l'}} \sum_{\substack{nm \\ n'm'}} \frac{\rho_{klk'l'}}{\sqrt{2^{k+l+k'+l'}}} \sqrt{\binom{k}{n}\binom{l}{m}\binom{k'}{n'}\binom{l'}{m'}}$$

$$\times |n, m, k-n, l-m\rangle\langle n', m', k'-n', l'-m'|. \quad (11)$$

The spin operators on the split condensate are defined as

$$S_j^x = a_j^\dagger b_j + b_j^\dagger a_j,$$
$$S_j^y = i(b_j^\dagger a_j - a_j^\dagger b_j),$$
$$S_j^z = a_j^\dagger a_j - b_j^\dagger b_j, \quad (12)$$

where $j \in \{1, 2\}$ labels the two condensates (either physical or virtual). These spin operators obey the bosonic commutation relations

$$[S^l, S^m] = 2i\epsilon_{lmn}S^n, \quad (13)$$

where ϵ_{lmn} is the Levi-Civita symbol and $l, m, n \in \{x, y, z\}$. The number operators for the two parts can be written as

$$\mathcal{N}_j = a_j^\dagger a_j + b_j^\dagger b_j, \quad (14)$$

where $j \in \{1, 2\}$.

C. Number fixing

The exciton-polariton condensate system is an open dissipative system and does not obey conservation of the total polariton number. In the context of atomic condensates, the total atom number N is assumed to be fixed for a single run of the experiment. Any relation that is derived for a fixed atom number (such as entanglement criteria) is not necessarily valid if the total particle number fluctuates. In order to deal

with this, we thus use an approach similar to that in Sec. II of Ref. [49] to map ρ^{sp} onto a fixed Hilbert space. Thus, we define the density matrix in the N sector as

$$\rho_N^{\text{sp}} = \frac{\Pi_N \rho^{\text{sp}} \Pi_N}{p_N}, \tag{15}$$

where

$$\Pi_N = \sum_{N_1=0}^{N} \sum_{k_1=0}^{N_1} \sum_{k_2=0}^{N-N_1} |k_1, N_1 - k_1, k_2, N - N_1 - k_2\rangle$$
$$\times \langle k_1, N_1 - k_1, k_2, N - N_1 - k_2| \tag{16}$$

is the projector on the N-particle subspace and N_1 is the number of polaritons in the first condensate. The probability of the N sector is defined as

$$p_N = \text{Tr}(\Pi_N \rho^{\text{sp}} \Pi_N), \tag{17}$$

which satisfies the relation

$$\sum_N p_N = 1. \tag{18}$$

Next, we define the expectation values of quantum operator $\mathcal{O}$ in fixed N sectors,

$$\langle \mathcal{O} \rangle_N \equiv \text{Tr}(\rho_N \mathcal{O}), \tag{19}$$

where ρ_N is the projection of ρ in a fixed N space and the subscript N refers to the fixed subspace. Therefore, the total polariton number would be

$$\langle \mathcal{N}_1 \rangle_N + \langle \mathcal{N}_2 \rangle_N = N. \tag{20}$$

The variance of operator $\mathcal{O}$ for the N sector is defined as

$$\text{Var}_N(\mathcal{O}) = \langle \mathcal{O}^2 \rangle_N - \langle \mathcal{O} \rangle_N^2. \tag{21}$$

The projector (16) involves a fixed polariton number N. However, the total polariton number collapses to fixed N_1 and N_2 after measurement. To define the projector in the fixed N_1, N_2 space ($N_2 = N - N_1$), we denote

$$\Pi_{N_1,N_2} = \sum_{k_1=0}^{N_1} \sum_{k_2=0}^{N_2} |k_1, N_1 - k_1, k_2, N_2 - k_2\rangle$$
$$\times \langle k_1, N_1 - k_1, k_2, N_2 - k_2|, \tag{22}$$

which gives a fixed particle number for the two halves. Thus, the expectation values for the operator $\mathcal{O}$ in this space can be written as

$$\langle \mathcal{O} \rangle_{N_1,N_2} \equiv \text{Tr}(\rho_{N_1,N_2} \mathcal{O}). \tag{23}$$

We then obtain the relation for the expectation value of $\mathcal{O}$ for the two types of number fixing:

$$\langle \mathcal{O} \rangle_N = \text{Tr}(\rho_N \mathcal{O})$$
$$= \sum_{N_1=0}^{N} \sum_{N_1'=0}^{N} \text{Tr}(\Pi_{N_1,N_2} \rho_N \Pi_{N_1',N_2'} \mathcal{O})$$

$$= \sum_{N_1=0}^{N} p_{N_1,N_2|N} \text{Tr}(\rho_{N_1,N_2} \mathcal{O})$$
$$= \sum_{N_1=0}^{N} p_{N_1,N_2|N} \langle \mathcal{O} \rangle_{N_1,N_2}, \tag{24}$$

where $p_{N_1,N_2|N}$ is the conditional probability and satisfies $\sum_{N_1}^{N} p_{N_1,N_2|N} = 1$, we assume $\mathcal{O}$ is a locally particle number conserving operator, and we use the fact that $\Pi_N^2 = \Pi_N$ and $\Pi_{N_1,N_2}^2 = \Pi_{N_1,N_2}$. The above relations will be useful for examining correlation-based entanglement detection criteria since they are often derived in the context of fixed N_1 and N_2 and we wish to relate them to number fluctuating averages.

III. NUMERICAL SIMULATION

A. Evaluation of expectation values

In simulating the master equation (1), a truncation is necessary since the full Hilbert space is unbounded. Therefore, we impose a cutoff N_{max}, which means that the number of bosons that occupy each mode is restricted to $k, l \in [0, N_{\text{max}}]$. Any states with $k, l > N_{\text{max}}$ are set to have zero amplitude. We note that the calculation of the effective spin still involves considering the truncation space within its context [49].

We then use (16) to project the states on fixed total number N. We note that, physically, such a projection is automatically done when any measurement is performed. In any entanglement detection procedure, one requires detection of the correlation between the two halves of the condensate. This involves detecting polaritons on the two sides of the condensate, and implicitly, this involves a number-fixing procedure. The density matrix (11) is defined in a large Hilbert space with four spin modes, a_1, b_1, a_2, and b_2. Due to the numerical overhead for directly calculating the split four-mode case, we calculate the expectation value of spin quantities $\mathcal{O}$ based on the original space before the splitting transformation, which contains only two modes. For example, the spin operators under this transformation will be written as

$$S_j^x = a_j^\dagger b_j + b_j^\dagger a_j \rightarrow \frac{1}{2}(a^\dagger b + a^\dagger \widetilde{b} + \widetilde{a}^\dagger b + \widetilde{a}^\dagger \widetilde{b})$$
$$+ \frac{1}{2}(b^\dagger a + b^\dagger \widetilde{a} + \widetilde{b}^\dagger a + \widetilde{b}^\dagger \widetilde{a}),$$

$$S_j^y = i(b_j^\dagger a_j - a_j^\dagger b_j) \rightarrow \frac{i}{2}(b^\dagger a + b^\dagger \widetilde{a} + \widetilde{b}^\dagger a + \widetilde{b}^\dagger \widetilde{a})$$
$$- \frac{i}{2}(a^\dagger b + a^\dagger \widetilde{b} + \widetilde{a}^\dagger b + \widetilde{a}^\dagger \widetilde{b}),$$

$$S_j^z = a_j^\dagger a_j - b_j^\dagger b_j \rightarrow \frac{1}{2}(a^\dagger a + a^\dagger \widetilde{a} + \widetilde{a}^\dagger a + \widetilde{a}^\dagger \widetilde{a})$$
$$- \frac{1}{2}(b^\dagger b + b^\dagger \widetilde{b} + \widetilde{b}^\dagger b + \widetilde{b}^\dagger \widetilde{b}), \tag{25}$$

where $j \in \{1, 2\}$ and we applied the inverse unitary transformation of the splitting procedure

$$a_1 \rightarrow \frac{1}{\sqrt{2}}(a + \widetilde{a}),$$

$$b_1 \rightarrow \frac{1}{\sqrt{2}}(b + \widetilde{b}),$$

$$a_2 \rightarrow \frac{1}{\sqrt{2}}(a - \widetilde{a}),$$

$$b_2 \rightarrow \frac{1}{\sqrt{2}}(b - \widetilde{b}). \tag{26}$$

The transformed spin operators involve both the original modes a and b as well as the unoccupied modes $\widetilde{a}$ and $\widetilde{b}$. Since we know that prior to the splitting operations the $\widetilde{a}$ and $\widetilde{b}$ annihilation operators are unoccupied, expectation values involving operators $\widetilde{a}$ and $\widetilde{b}$ will be zero. For example, expectation values of the local modes are

$$\langle S_j^x \rangle_N = \frac{1}{2}\langle a^\dagger b + b^\dagger a \rangle_N,$$

$$\langle S_j^y \rangle_N = \frac{i}{2}\langle b^\dagger a - a^\dagger b \rangle_N,$$

$$\langle S_j^z \rangle_N = \frac{1}{2}\langle a^\dagger a - b^\dagger b \rangle_N, \tag{27}$$

where $j \in \{1, 2\}$. For second-order spin correlations, we have

$$\langle S_1^x S_2^x \rangle_N = \frac{1}{4}\langle a^\dagger b a^\dagger b + a^\dagger b b^\dagger a - a^\dagger a + b^\dagger a a^\dagger b - b^\dagger b + b^\dagger a b^\dagger a \rangle_N,$$

$$\langle S_1^y S_2^y \rangle_N = \frac{1}{4}\langle a^\dagger b b^\dagger a - a^\dagger a - a^\dagger b a^\dagger b - b^\dagger a b^\dagger a + b^\dagger a a^\dagger b - b^\dagger b \rangle_N,$$

$$\langle S_1^z S_2^z \rangle_N = \frac{1}{4}\langle a^\dagger a a^\dagger a - a^\dagger a - a^\dagger a b^\dagger b - b^\dagger b a^\dagger a + b^\dagger b b^\dagger b - b^\dagger b \rangle_N, \tag{28}$$

where we used the commutation relation $[\widetilde{a}, \widetilde{a}^\dagger] = [\widetilde{b}, \widetilde{b}^\dagger] = 1$.

The elements of density matrix (11) can also be obtained from the original space, which can be calculated by

$$\langle k_1, l_1, k_2, l_2 | \rho^{\mathrm{sp}} | k_1', l_1', k_2', l_2' \rangle$$

$$= \frac{1}{\sqrt{k_1! l_1! k_2! l_2! k_1'! l_1'! k_2'! l_2'!}}$$

$$\times \langle 0 | a_1^{k_1} b_1^{l_1} a_2^{k_2} b_1^{l_2} \rho^{\mathrm{sp}} (a_1^\dagger)^{k_1'} (b_1^\dagger)^{l_1'} (a_2^\dagger)^{k_2'} (b_1^\dagger)^{l_2'} | 0 \rangle$$

$$\rightarrow \frac{1}{\sqrt{k_1! l_1! k_2! l_2! k_1'! l_1'! k_2'! l_2'!}} \frac{1}{\sqrt{2}^{k_1+l_1+k_2+l_2+k_1'+l_1'+k_2'+l_2'}}$$

$$\times \langle 0 | a^{k_1+k_2} b^{l_1+l_2} \rho (a^\dagger)^{k_1'+k_2'} (b^\dagger)^{l_1'+l_2'} | 0 \rangle, \tag{29}$$

where, again, we used the inverse unitary transformation (26).

In the noninteracting limit ($U/\gamma = V/\gamma = 0$), each N sector corresponds to a spin-coherent state $|1/\sqrt{2}, 1/\sqrt{2}\rangle_1 \otimes |1/\sqrt{2}, 1/\sqrt{2}\rangle_2$ in the pump regime, where $\theta_a = \theta_b = 0$ and $\Delta = 0$ after spin mapping [49], where we define the spin-coherent state as

$$|\alpha, \beta\rangle = \frac{1}{\sqrt{N!}}(\alpha a^\dagger + \beta b^\dagger)^N | 0 \rangle$$

$$= \sum_k \sqrt{\binom{N}{k}} \alpha^k \beta^{N-k} | k, N-k \rangle. \tag{30}$$

For the initial state that is polarized in the S^x direction, we find that

$$\langle S_1^x \rangle_N = \frac{1}{2^N} \sum_{N_1} \binom{N}{N_1} N_1 = \frac{N}{2}, \tag{31}$$

$$\langle S_2^x \rangle_N = \frac{1}{2^N} \sum_{N_2} \binom{N}{N_2} N_2 = \frac{N}{2}. \tag{32}$$

Hence, for each chosen N sector, the average number of polaritons for the two parts is $N/2$, which indicates the equivalence of the calculations in the large space and in the split procedure.

B. Effective entangling Hamiltonian

To show the effect of one-axis twisting in this split procedure, we project the total spin operator S^z onto the fixed N_1, N_2 space by using (22):

$$\Pi_{N_1,N_2} S^z \Pi_{N_1,N_2} = \Pi_{N_1,N_2} a^\dagger a \Pi_{N_1,N_2} - \Pi_{N_1,N_2} b^\dagger b \Pi_{N_1,N_2}$$

$$= \frac{1}{2}\Pi_{N_1,N_2}(a_1^\dagger a_1 - b_1^\dagger b_1 + a_2^\dagger a_2 - b_2^\dagger b_2)$$

$$\times \Pi_{N_1,N_2}$$

$$+ \frac{1}{2}\Pi_{N_1,N_2}(a_1^\dagger a_2 + a_2^\dagger a_1 - b_1^\dagger b_2 - b_2^\dagger b_1)$$

$$\times \Pi_{N_1,N_2}$$

$$\rightarrow \Pi_{N_1,N_2}(a_1^\dagger a_1 - b_1^\dagger b_1 + a_2^\dagger a_2 - b_2^\dagger b_2)\Pi_{N_1,N_2}$$

$$= \Pi_{N_1,N_2}(S_1^z + S_2^z)\Pi_{N_1,N_2}, \tag{33}$$

where the cross terms return zero for a fixed number N. Using the above result, we then obtain

$$\Pi_{N_1,N_2}(S^z)^2 \Pi_{N_1,N_2} = (\Pi_{N_1,N_2} S^z \Pi_{N_1,N_2})^2$$

$$\rightarrow \Pi_{N_1,N_2}(S_1^z + S_2^z)^2 \Pi_{N_1,N_2}$$

$$= \Pi_{N_1,N_2}((S_1^z)^2 + 2S_1^z S_2^z + (S_2^z)^2)\Pi_{N_1,N_2}, \tag{34}$$

where we applied the relations $\Pi_{N_1,N_2}^2 = \Pi_{N_1,N_2}$ and $[\Pi_{N_1,N_2}, S^z] = 0$. Thus, the effective spin of the squeezing-generation operator S_z^2 in one single-polariton condensate in a fixed N_1, N_2 subspace corresponds to the case with two spatial BECs as $(S^z)^2 \rightarrow (S_1^z)^2 + 2S_1^z S_2^z + (S_2^z)^2$. This shows that we expect squeezing on each condensate individually due to the terms $(S_1^z)^2$ and $(S_2^z)^2$, and the term $2S_1^z S_2^z$ generates entanglement between two condensates. This is similar to the one-axis, two-spin squeezing Hamiltonian, which produces entanglement with a fractal time dependence [52,53].

IV. ENTANGLEMENT DETECTION

A. Logarithmic negativity

Logarithmic negativity is an entanglement monotone that is used to quantify the bipartite entanglement in mixed states [54–56]. It is defined as

$$E(\rho_N^{\mathrm{sp}}) = \log_2 ||(\rho_N^{\mathrm{sp}})^{T_2}|| = \log_2 \sum_i |\lambda_i|, \tag{35}$$

where $(\rho_N^{\mathrm{sp}})^{T_2}$ is the partial transpose of the second polariton BEC density matrix, $||\mathcal{X}||$ is the Schatten 1-norm of $\mathcal{X}$,
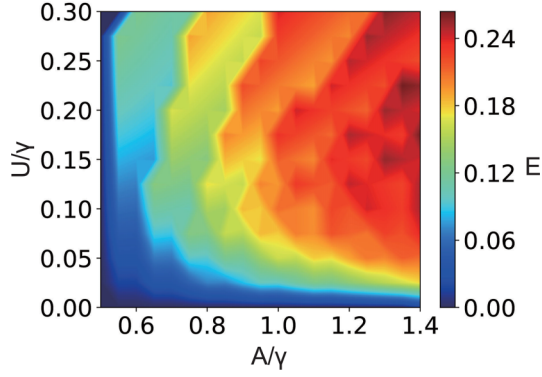
FIG. 3. The logarithmic negativity (35) as a function of pump rate A/γ and the nonlinear S_z^2 interaction parameter U/γ. Common parameters are $V/\gamma = 0$, $\theta_a = \theta_b = 0$, and $N_{\max} = 10$.

and $|\lambda_i|$ is the absolute value of the eigenvalues of $(\rho_N^{\rm sp})^{T_2}$. The range of E is from zero to the maximum value $E_{\max} = \log_2(N/2 + 1)$, where in the maximally entangled case $N_1 = N_2 = N/2$. We note that this result involves only the N sector which has the maximum p_N for the particular parameter set that we choose, i.e., the most likely measured N sector.

In Fig. 3, we examine the logarithmic negativity, where we show (35) as a function of the pumping rate A/γ and the squeezing-interaction parameter U/γ. We find that $E = 0$ for a spin-coherent state ($U/\gamma = 0$) and $E > 0$ when both $U/\gamma, A/\gamma > 0$, as expected. The tendency of the growth of E with A/γ and U/γ is clearly seen. We note that large N needs less time to reach the same squeezing level, as expected from the optimal squeezing time $\propto 1/N^{2/3}$ for one-axis squeezing [57,58]. Larger pumping and interaction correspond to a higher level of squeezing, giving rise to more entanglement in our system. We thus expect that entanglement should be present in the current polariton system at steady state for a large pumping rate and high-Q cavity regime [49]. Concretely, this would mean parameters corresponding to $1/\gamma > 30$ ps and $U/\gamma > 0.3$.

B. Correlation-based criteria

While a nonzero logarithmic negativity gives an unambiguous signal of entanglement, it may be difficult in practice to detect it in experiment due to the need for full density-matrix tomography. Thus, experimental limitations may require the use of alternative measures that are better suited to the available measurements. Several correlation-based entanglement detectors are available. The more sensitive detectors are the expectation values of total spin operators. The first one we consider is the Giovannetti-Mancini-Vitali-Tombesi (GMVT) criterion [59], which states that for any separable state

$$\frac{\sqrt{{\rm Var}_N(g_y S_1^y - S_2^y){\rm Var}_N(g_z S_1^z + S_2^z)}}{|g_y g_z|(|\langle S_1^x \rangle_N| + |\langle S_2^x \rangle_N|)} \geqslant 1, \quad (36)$$

where g_y and g_z are free parameters to minimize the left-hand side. The inequality (36) is true for all separable states. Hence, a violation of the inequality indicates that the state must be entangled. In our case we choose $g_y = g_z = 1$. The second criterion is the Duan-Giedke-Cirac-Zoller (DGCZ) criterion
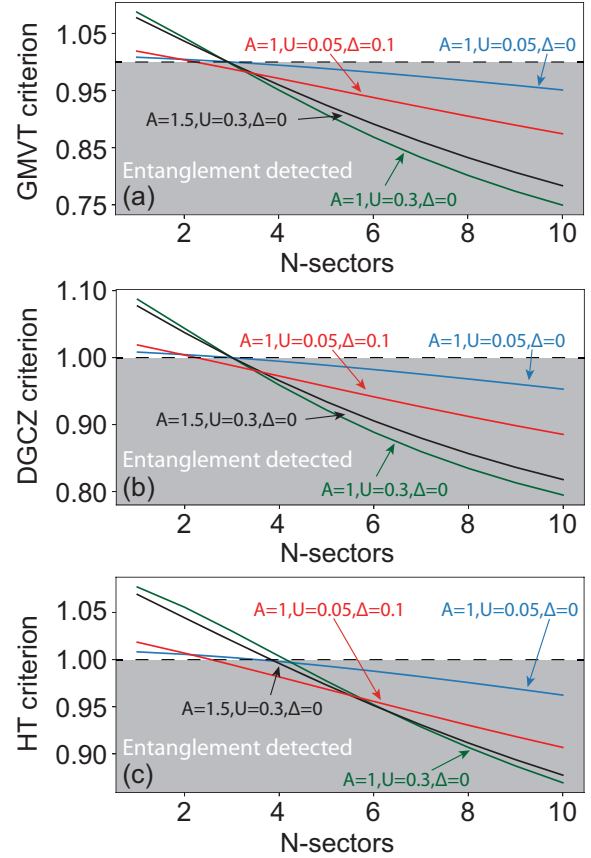

FIG. 4. Entanglement criteria for the split polariton condensate system at steady state. Criteria (36), (37), and (38) versus N sectors are calculated in (a)–(c), respectively. The main experimental parameters A/γ, U/γ, and Δ/γ are as marked. The shaded regions indicate the presence of entanglement. The indicated values are in units of γ. Common parameters are $V/\gamma = 0$, $\theta_a = \theta_b = 0$, and $N_{\max} = 10$.

[60], which is valid for any separable state

$$\frac{{\rm Var}_N(S_1^y - S_2^y) + {\rm Var}_N(S_1^z + S_2^z)}{2(|\langle S_1^x \rangle_N| + |\langle S_2^x \rangle_N|)} \geqslant 1. \quad (37)$$

The third criterion is the Hofmann-Takeuchi (HT) criterion [61], which is valid for any separable state

$$\frac{{\rm Var}_N(S_1^x + S_2^x) + {\rm Var}_N(S_1^y - S_2^y) + {\rm Var}_N(S_1^z + S_2^z)}{2(\langle \mathcal{N}_1 \rangle_N + \langle \mathcal{N}_2 \rangle_N)} \geqslant 1, \quad (38)$$

where N is the total polariton number of the N sector. The above inequalities have been converted from their fixed N_1, N_2 relations to a fixed N through an averaging procedure. We note that the average variance of the operator $\mathcal{O}$ in the fixed N_1, N_2 space is either equal to or less than the variance defined using N sectors, denoted by ${\rm Var}_N(\mathcal{O})$ (see Appendix A). Furthermore, the average expectation values are equal to $\langle \mathcal{O} \rangle_N$ (see Appendix B). Therefore, the violation of inequalities (36)–(38) indicates the presence of entanglement within each N sector.

Figures 4(a)–4(c) show the three criteria as a function of the N sectors. The first thing that we notice is the similar behavior of GMVT and DGCZ criteria. The curves show that
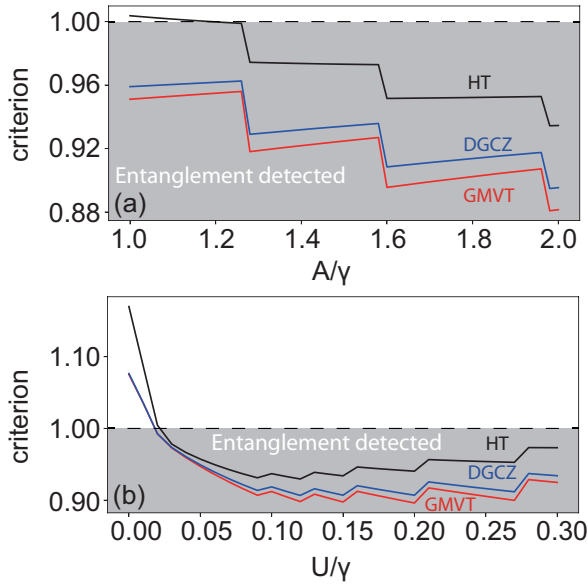
FIG. 5. Entanglement criteria (36), (37), and (38) for the split polariton condensate system at steady state as a function of (a) pump rate A/γ and (b) interaction parameter U/γ. The three entanglement criteria are as marked. The N sectors are chosen by the maximum p_N for each parameter. The shaded regions indicate the presence of entanglement. Parameters are (a) $U/\gamma = 0.3$ and (b) $A/\gamma = 1.5$. Common parameters are $\Delta/\gamma = 0$, $V/\gamma = 0$, $\theta_a = \theta_b = 0$, and $N_{\max} = 10$.

the former detects entanglement in a wider range than the latter. In Fig. 4(a), we see that for experimentally reasonable parameter choices, for larger A/γ and small Δ/γ, the entanglement criteria decrease monotonically with N. This shows that more squeezing is present for larger N, which was observed from the Q functions and squeezing parameters in Ref. [49]. Comparing the different parameters U/γ, we find that we obtain a larger violation level in a high-Q cavity, where the larger U/γ yields more squeezing. We note that the value of these nonseparability criteria does not necessarily mean more entanglement and indicates solely the presence of entanglement [62]. It may, however, be experimentally advantageous to have a larger violation in order to more easily detect entanglement. Further, we show that the small detuning can increase the level of violation considerably. Depending upon the N sector examined, in some cases increasing the pump A/γ does not necessarily lead to an increased violation. We find a threshold in the N sector, where below the threshold a larger pump rate A/γ tends to increase violation, while above the threshold it decreases. For example, under HT criterion in Fig. 4(c), the threshold is $N \approx 6$.

Figure 5(a) shows a "staircase" dependence of the GMVT, DGCZ, and HT criteria. The staircase dependence is observed because we consider the most likely N sector to be measured, and with increasing A/γ or U/γ this changes. For example, at $A/\gamma \sim 1.25$, the violation level suddenly decreases due to the change in the N sector; then the violation level slightly decreases. What this shows is that while increasing A/γ can slightly degrade the level of violation within a fixed N sector, a larger pump can also change the most probable N sector,

which can lead to an improvement in the level of violation. In experiments, typically, a larger pump rate is easily achieved, and a large violation is easier to observe; thus, the most reachable regime is the higher A/γ. In Fig. 5(b) we show these three criteria versus the interaction parameter U/γ. We see that below the threshold $U/\gamma \sim 0.09$, the violation level improves monotonically but then saturates and again has a staircase dependence due to the changes in the N sector. Therefore, to obtain a larger violation level, a moderate interaction U/γ may be sufficient to obtain an optimized level of violation.

V. CONCLUSION

In this work we theoretically proposed a method of generating spatially separated entanglement at steady state in a spinor exciton-polariton condensate and gave two ways of realizing the experimental setup. In the first approach, the polaritons are physically split in a coherent fashion by increasing an external potential, for example. The second approach involves virtually splitting the polariton condensate into two halves by examining a spatially resolved near-field image of entanglement in the polariton condensate. Equivalent results were obtained for these two approaches in the ideal case. Technically, the virtual split is much easier to achieve than the physical split since such extra manipulations may involve additional sources of decoherence. However, the physical split is more in line with the notion of two separated entangled condensates, as experimentally achieved in Ref. [32] recently. The initial formation of the condensate can be attributed to one-axis spin-squeezing interaction between the polariton modes. This type of interaction leads to entanglement generation between all polaritons in the system. The formation of entanglement can be attributed to the cross term $2S_1^z S_2^z$ (34). By examining and comparing the logarithmic negativity, GMVT, DGCZ, and HT criteria in various regimes, we showed such entanglement can be detected between the two condensates. The entanglement can be improved with increasing pump rate A/γ. We also found that a small detuning Δ/γ can enhance entanglement. Further, one may obtain an optimal entanglement level by adjusting the interaction parameter U/γ. To date, there has not been any report of entanglement generation in a polaritonic system. Several experiments with atomic BECs have been performed, both at the single-BEC level to demonstrate entanglement and between two physically separated atomic BECs. Due to the controllability of the polariton condensate, there is an opportunity to experimentally realize some of these milestones in the near future.

APPENDIX A: DERIVATION OF THE VARIANCE AVERAGE IN THE FIXED N_1, N_2 SPACE

The definition of the variance average of a quantum operator $\mathcal{O}$ is

$$\sum_{N_1=0}^{N} p_{N_1,N_2|N} \mathrm{Var}_{N_1,N_2}(\mathcal{O})$$

$$= \sum_{N_1=0}^{N} p_{N_1,N_2|N} \langle \mathcal{O}^2 \rangle_{N_1,N_2} - \sum_{N_1=0}^{N} p_{N_1,N_2|N} \langle \mathcal{O} \rangle_{N_1,N_2}^2. \quad \text{(A1)}$$

Using the Cauchy-Schwarz inequality [60], we find

$$\sum_{N_1=0}^{N} p_{N_1,N_2|N} \mathrm{Var}_{N_1,N_2}(\mathcal{O})$$

$$\leqslant \sum_{N_1=0}^{N} p_{N_1,N_2|N} \langle \mathcal{O}^2 \rangle_{N_1,N_2} - \left(\sum_{N_1=0}^{N} p_{N_1,N_2|N} |\langle \mathcal{O} \rangle_{N_1,N_2}| \right)^2$$

$$\leqslant \sum_{N_1=0}^{N} p_{N_1,N_2|N} \langle \mathcal{O}^2 \rangle_{N_1,N_2} - \left(\sum_{N_1=0}^{N} p_{N_1,N_2|N} \langle \mathcal{O} \rangle_{N_1,N_2} \right)^2. \quad \text{(A2)}$$

By substituting $\langle \mathcal{O}^2 \rangle_{N_1,N_2}$ and $\langle \mathcal{O} \rangle_{N_1,N_2}^2$ with $\langle \mathcal{O}^2 \rangle_N$ and $\langle \mathcal{O} \rangle_N^2$ (24), we have

$$\sum_{N_1=0}^{N} p_{N_1,N_2|N} \mathrm{Var}_{N_1,N_2}(\mathcal{O}) \leqslant \mathrm{Var}_N(\mathcal{O}). \quad \text{(A3)}$$

Replacing $\mathcal{O}$ with $S_1^x + S_2^x$, $S_1^y - S_2^y$, and $S_1^z + S_2^z$, we obtain the relations in (36)–(38), respectively.

APPENDIX B: DERIVATION OF THE AVERAGE OF THE EXPECTATION VALUES IN THE FIXED N_1, N_2 SPACE

The definition of the average of the expectation values of a quantum operator $\mathcal{O}$ is

$$\sum_{N_1=0}^{N} p_{N_1,N_2|N} \langle \mathcal{O} \rangle_{N_1,N_2}. \quad \text{(B1)}$$

By using the relations (24) we have

$$\sum_{N_1=0}^{N} p_{N_1,N_2|N} \langle \mathcal{O} \rangle_{N_1,N_2} = \langle \mathcal{O} \rangle_N. \quad \text{(B2)}$$

Replacing $\mathcal{O}$ with S_1^x, S_2^x, $\mathcal{N}_1$, and $\mathcal{N}_2$, we obtain the relations in (36)–(38), respectively.

[1] V. Vedral, M. B. Plenio, M. A. Rippin, and P. L. Knight, Phys. Rev. Lett. **78**, 2275 (1997).

[2] V. Vedral, Nat. Phys. **10**, 256 (2014).

[3] C. H. Bennett, G. Brassard, C. Crépeau, R. Jozsa, A. Peres, and W. K. Wootters, Phys. Rev. Lett. **70**, 1895 (1993).

[4] J. Lee, H. Min, and S. D. Oh, Phys. Rev. A **66**, 052318 (2002).

[5] N. Gisin, G. Ribordy, W. Tittel, and H. Zbinden, Rev. Mod. Phys. **74**, 145 (2002).

[6] J. Yin, Y.-H. Li, S.-K. Liao, M. Yang, Y. Cao, L. Zhang, J.-G. Ren, W.-Q. Cai, W.-Y. Liu, S.-L. Li *et al.*, Nature (London) **582**, 501 (2020).

[7] A. K. Ekert, Phys. Rev. Lett. **67**, 661 (1991).

[8] V. Giovannetti, S. Lloyd, and L. Maccone, Nat. Photonics **5**, 222 (2011).

[9] L. Pezzè, A. Smerzi, M. K. Oberthaler, R. Schmied, and P. Treutlein, Rev. Mod. Phys. **90**, 035005 (2018).

[10] H. Krauter, D. Salart, C. A. Muschik, J. M. Petersen, H. Shen, T. Fernholz, and E. S. Polzik, Nat. Phys. **9**, 400 (2013).

[11] S. Kotler, G. A. Peterson, E. Shojaee, F. Lecocq, K. Cicak, A. Kwiatkowski, S. Geller, S. Glancy, E. Knill, R. W. Simmonds *et al.*, Science **372**, 622 (2021).

[12] K. Lange, J. Peise, B. Lücke, I. Kruse, G. Vitagliano, I. Apellaniz, M. Kleinmann, G. Tóth, and C. Klempt, Science **360**, 416 (2018).

[13] P. Kunkel, M. Prüfer, H. Strobel, D. Linnemann, A. Frölian, T. Gasenzer, M. Gärttner, and M. K. Oberthaler, Science **360**, 413 (2018).

[14] M. Fadel, T. Zibold, B. Décamps, and P. Treutlein, Science **360**, 409 (2018).

[15] R. Schmied, J.-D. Bancal, B. Allard, M. Fadel, V. Scarani, P. Treutlein, and N. Sangouard, Science **352**, 441 (2016).

[16] T. Berrada, S. van Frank, R. Bücker, T. Schumm, J.-F. Schaff, and J. Schmiedmayer, Nat. Commun. **4**, 2077 (2013).

[17] J. Estève, C. Gross, A. Weller, S. Giovanazzi, and M. K. Oberthaler, Nature (London) **455**, 1216 (2008).

[18] H. Deng, H. Haug, and Y. Yamamoto, Rev. Mod. Phys. **82**, 1489 (2010).

[19] J. Kasprzak, M. Richard, S. Kundermann, A. Baas, P. Jeambrun, J. M. J. Keeling, F. M. Marchetti, M. H. Szymańska, R. André, J. L. Staehli *et al.*, Nature (London) **443**, 409 (2006).

[20] J. Keeling and N. G. Berloff, Contemp. Phys. **52**, 131 (2011).

[21] T. Byrnes, N. Y. Kim, and Y. Yamamoto, Nat. Phys. **10**, 803 (2014).

[22] H. Deng, G. Weihs, C. Santori, J. Bloch, and Y. Yamamoto, Science **298**, 199 (2002).

[23] R. Balili, V. Hartwell, D. Snoke, L. Pfeiffer, and K. West, Science **316**, 1007 (2007).

[24] M. Wouters and I. Carusotto, Phys. Rev. A **76**, 043807 (2007).

[25] J. Bloch, I. Carusotto, and M. Wouters, Nat. Rev. Phys. **4**, 470 (2022).

[26] S. Christopoulos, G. B. H. v. Högersthal, A. J. D. Grundy, P. G. Lagoudakis, A. V. Kavokin, J. J. Baumberg, G. Christmann, R. Butté, E. Feltin, J.-F. Carlin, and N. Grandjean, Phys. Rev. Lett. **98**, 126405 (2007).

[27] J. J. Baumberg, A. V. Kavokin, S. Christopoulos, A. J. D. Grundy, R. Butté, G. Christmann, D. D. Solnyshkov, G. Malpuech, G. Baldassarri Höger von Högersthal, E. Feltin, J.-F. Carlin, and N. Grandjean, Phys. Rev. Lett. **101**, 136409 (2008).

[28] S. Kéna-Cohen and S. R. Forrest, Nat. Photonics **4**, 371 (2010).

[29] T. Guillet, M. Mexis, J. Levrat, G. Rossbach, C. Brimont, T. Bretagnon, B. Gil, R. Butté, N. Grandjean, L. Orosz *et al.*, Appl. Phys. Lett. **99**, 161104 (2011).

[30] J. D. Plumhof, T. Stöferle, L. Mai, U. Scherf, and R. F. Mahrt, Nat. Mater. **13**, 247 (2014).

[31] F. Chen, H. Li, H. Zhou, S. Luo, Z. Sun, Z. Ye, F. Sun, J. Wang, Y. Zheng, X. Chen, H. Xu, H. Xu, T. Byrnes, Z. Chen, and J. Wu, Phys. Rev. Lett. **129**, 057402 (2022).

[32] P. Colciaghi, Y. Li, P. Treutlein, and T. Zibold, Phys. Rev. X **13**, 021031 (2023).

[33] Y. Jing, M. Fadel, V. Ivannikov, and T. Byrnes, New J. Phys. **21**, 093038 (2019).

[34] P. Treutlein, T. W. Hänsch, J. Reichel, A. Negretti, M. A. Cirone, and T. Calarco, Phys. Rev. A **74**, 022312 (2006).

[35] J. Kitzinger, M. Chaudhary, M. Kondappan, V. Ivannikov, and T. Byrnes, Phys. Rev. Res. **2**, 033504 (2020).

[36] S. Idlas, L. Domenzain, R. Spreeuw, and T. Byrnes, Phys. Rev. A **93**, 022319 (2016).

[37] A. N. Pyrkov and T. Byrnes, New J. Phys. **15**, 093019 (2013).

[38] O. Pettersson and T. Byrnes, Phys. Rev. A **95**, 043817 (2017).

[39] A. Abdelrahman, T. Mukai, H. Häffner, and T. Byrnes, Opt. Express **22**, 3501 (2014).

[40] D. Rosseau, Q. Ha, and T. Byrnes, Phys. Rev. A **90**, 052315 (2014).

[41] M. I. Hussain, E. O. Ilo-Okeke, and T. Byrnes, Phys. Rev. A **89**, 053607 (2014).

[42] T. Boulier, M. Bamba, A. Amo, C. Adrados, A. Lemaitre, E. Galopin, I. Sagnes, J. Bloch, C. Ciuti, E. Giacobino *et al.*, Nat. Commun. **5**, 3260 (2014).

[43] N. Y. Kim, C.-W. Lai, S. Utsunomiya, G. Roumpos, M. Fraser, H. Deng, T. Byrnes, P. Recher, N. Kumada, T. Fujisawa *et al.*, Phys. Status Solidi B **245**, 1076 (2008).

[44] E. Estrecho, Nat. Rev. Phys. **3**, 536 (2021).

[45] Y. Wu, J. Duan, W. Ma, Q. Ou, P. Li, P. Alonso-González, J. D. Caldwell, and Q. Bao, Nat. Rev. Phys. **4**, 578 (2022).

[46] M. C. Tichy, P. A. Bouvrie, and K. Mølmer, Phys. Rev. Lett. **109**, 260403 (2012).

[47] P. A. Bouvrie, M. C. Tichy, and K. Mølmer, Phys. Rev. A **94**, 053624 (2016).

[48] P. A. Bouvrie, E. Cuestas, I. Roditi, and A. P. Majtey, Phys. Rev. A **99**, 063601 (2019).

[49] J. Feng, E. O. Ilo-Okeke, A. N. Pyrkov, A. Askitopoulos, and T. Byrnes, Phys. Rev. A **104**, 013318 (2021).

[50] A. F. Adiyatullin, M. D. Anderson, H. Flayac, M. T. Portella-Oberli, F. Jabeen, C. Ouellet-Plamondon, G. C. Sallen, and B. Deveaud, Nat. Commun. **8**, 1329 (2017).

[51] H. Takesue and K. Inoue, Phys. Rev. A **70**, 031802(R) (2004).

[52] T. Byrnes, Phys. Rev. A **88**, 023609 (2013).

[53] H. Kurkjian, K. Pawłowski, A. Sinatra, and P. Treutlein, Phys. Rev. A **88**, 043605 (2013).

[54] M. B. Plenio, Phys. Rev. Lett. **95**, 090503 (2005).

[55] G. Vidal and R. F. Werner, Phys. Rev. A **65**, 032314 (2002).

[56] G. Adesso and F. Illuminati, Phys. Rev. A **72**, 032334 (2005).

[57] M. Kitagawa and M. Ueda, Phys. Rev. A **47**, 5138 (1993).

[58] T. Byrnes and E. O. Ilo-Okeke, *Quantum Atom Optics: Theory and Applications to Quantum Technology* (Cambridge University Press, Cambridge, 2021).

[59] V. Giovannetti, S. Mancini, D. Vitali, and P. Tombesi, Phys. Rev. A **67**, 022320 (2003).

[60] L.-M. Duan, G. Giedke, J. I. Cirac, and P. Zoller, Phys. Rev. Lett. **84**, 2722 (2000).

[61] H. F. Hofmann and S. Takeuchi, Phys. Rev. A **68**, 032103 (2003).

[62] M. Isoard, N. Milazzo, N. Pavloff, and O. Giraud, Phys. Rev. A **104**, 063302 (2021).